Available online at www.sciencedirect.com

jmr&t Journal of Materials Research and Technology

https://www.journals.elsevier.com/journal-of-materials-research-and-technology

Original Article

Transformations with inhomogeneous nucleation and growth velocity

Mariana Sizenando Lyrio[a,*], *Gabriella Maria Silveira de Sá*[a], *Harison da Silva Ventura*[a], *Weslley Luiz da Silva Assis*[a], *Elena Villa*[b], *Paulo Rangel Rios*[a]

[a] *Universidade Federal Fluminense, Escola de Engenharia Industrial Metalúrgica de Volta Redonda, Av. dos Trabalhadores, 420, Volta Redonda, RJ, 27255-125, Brazil*

[b] *University of Milan, Department of Mathematics, via Saldini 50, 20133 Milano, Italy*

ARTICLE INFO

Article history:
Received 28 April 2020
Accepted 17 June 2020

Keywords:
Computer simulation
Microstructure
Phase transformations
Nucleation and growth transformations
Analytical methods

ABSTRACT

The major part of solid-state transformations modeling has concentrated on transformations taking place from a homogeneous matrix. Nonetheless, there are situations in which one finds an inhomogeneous matrix. An example is the recrystallization of metals subjected to an inhomogeneous deformation. If the recrystallization takes place in the regions where the stored energy of cold work is high, one has both a higher number of nuclei and faster growth velocity than in the region where the stored energy is low. In this work, we conduct computer simulations of transformations of a matrix possessing inhomogeneous nucleation and growth. We compare the computer simulations with an analytical solution that considers at the same time both the variation of the number of nuclei and the velocity. These results are compared with results obtained when only inhomogeneous nucleation is considered, whereas the velocity is kept constant throughout the matrix. For the number of nuclei and velocity gradients used here the main simulation results were: a) the inhomogeneous velocity does have a substantial effect on the transformation kinetics and microstructural evolution, b) the inhomogeneous distribution of nuclei has a more significant impact on the microstructure than an inhomogeneous distribution of velocity

1. Introduction

Solid-state transformations very often take place by nucleation of a new region and its subsequent growth. Extant models of solid-state transformations usually take a homogeneous and isotropic matrix as their starting point. When the material is a polycrystal, the transformation may initiate at the grain boundaries, but still, the matrix is isotropic.

The methodology proposed by Johnson-Mehl, Avrami, and Kolmogorov [1–5], the so-called JMAK theory, contains, to this day, the basic ideas that one uses to model nucleation and growth transformation from a homogeneous and isotropic matrix. Typically, JMAK is associated with isothermal transformation. By contrast, Wang et al. [6] work is a significant

* *Corresponding author.*
E-mail: mlyrio@id.uff.br (M.S. Lyrio).

https://doi.org/10.1016/j.jmrt.2020.06.064

contribution to make JMAK's equations also applicable to non-isothermal transformations [6]. JMAK theory does not go into the physical mechanisms of nucleation and growth. Instead, JMAK theory prescribes the nucleation rate, the spatial position of the nuclei as well as the growth velocity of the transforming regions.

JMAK theory, together with its developments and extensions, still finds widespread application to transformations in both metallic and nonmetallic materials. JMAK theory has been applied beyond first-order transitions to situations in which nucleation and growth have a phenomenological value. As a result, one can see the JMAK theory employed to describe a broad spectrum of transformations. JMAK theory can be applied to austenite-to-perlite transformation [2], austenite-to-ferrite with or without applied stress [7,8], recrystallization [9], abnormal grain growth in $BaTiO_3$ [10,11], martensite "spread" [12,13], polymer crystallization [14], and even to Medical research to describe the growth of tumors [15].

In their original work, JMAK derived two equations. In both cases, the velocity was constant, and the regions were spherical. The difference was how the nucleation proceeded. They derived the first equation supposing that nucleation took place at a constant rate. By contrast, in the derivation of the second equation, JMAK supposed that all the nucleation started, i. e, "saturated," early in the transformation, and no nucleation took place afterward. This second case is the so-called "site-saturated," which we will focus on this work. It is worthy of note that nuclei were uniform randomly distributed in space in both cases.

The well-known expression for the site-saturated case is given here for convenience, as this work will focus on site-saturated nucleation

$$\mathbf{V_V}(t) = 1 - \exp\left(\frac{-4\pi}{3}\lambda G^3 t^3\right) \tag{1}$$

In Eq. 1 $\mathbf{V_V}(t)$ is the volume fraction transformed as a function of time, t. The growth velocity is a constant, G. The number of nuclei per unit of volume is λ. It is worthy of note that nuclei were uniform randomly distributed in space in both cases. Eq. 1 applies to the description of a transformation on a homogeneous matrix.

In practice, many situations arise that differ from JMAK's original assumptions. Perhaps the simpler deviation is that the velocity might not be constant during transformation. In this particular case, JMAK findings can be easily adapted by introducing, for example, a time-dependent velocity. JMAK methodology may not be so straightforward in other cases. There might be situations in which the nucleation rate and growth rate may not be simple or even possible to determine. Avrami herself recognized that deviations from their assumptions could take place and proposed a generalized form of her equation that is known to this day as Avrami's equation [16]:

$$\mathbf{V_V}(t) = 1 - \exp\left(-kt^n\right) \tag{2}$$

where k and n are adjustable parameters. This equation has been widely used to phenomenologically model transformations for which it is difficult to assess their nucleation and growth rates. An alternative to Avrami's expression has been recently proposed [17].

One might say that JMAK's work gave birth to two distinct approaches to formal kinetics. On the one hand, researchers tried to derive JMAK-like analytical expressions for transformation kinetics by making different assumptions about nucleation and growth. On the other hand, researchers took Eq. 2 as their starting point. Expanding on Eq. 2 and the concepts of JMAK, the researchers developed formal methodologies that are particularly suitable for situations in which it is hard to obtain detailed information about nucleation and growth. There are numerous papers based on the latter approach. A comprehensive review of this methodology up to 2007 can be found in Liu et al. [18]. From 2007 to this day, more work has been done on this subject. Song et al. [19,20] used the methodology described in Liu et al. to develop expressions for anisotropic growth. It is also worth mentioning a series of papers by Liu et al. [21–23] applying Liu et al. methodology [18] to quantify a variety of transformations. Our summary cannot be exhaustive. A full review of this exciting branch of formal kinetics is beyond the scope of this paper.

These diverse approaches are not mutually exclusive, and each has its importance to the theory and practice of transformations in solids, depending on the problem to be solved.

Returning to JMAK's approach, Rios and Villa [24–26] contain a brief review of exact extensions and equations describing a diversity of nuclei locations in space.

In industry, one often has inhomogeneities that arise during the production process. These could be, for example, a temperature gradient [14,27] or a deformation gradient [28–33]. This microstructural gradient can be generated by pre-deformation in the material. An old [34] technique is indentation. Through the spherical indentation applied to the material at room temperature, a deformation gradient is established. In this way, recrystallization can be correlated with the amount of strain applied.

It is necessary to account for both inhomogeneous nucleation and inhomogeneous velocity to obtain an equation suitable for modeling the transformation in an inhomogeneous matrix.

Rios and Villa [24] generalized Eq. 1 for inhomogeneous nucleation. The point to do this is to recognize that ünifórm randomlyÏocated nuclei may be more rigorously described by a homogeneous Poisson point process. Using modern concepts from stochastic geometry [25], Rios and Villa obtained

$$V_V(t, x) = 1 - \exp\left(-\frac{4\pi}{3}\lambda(x) G^3 t^3\right) \tag{2}$$

In Eq. 2 instead of a volume fraction as in Eq.1 one now has a *mean volume density*, $V_V(t, x)$. The mean number of nuclei in a bounded region $A \subset \mathbb{R}^3$ is now given by $\int_{A(t,x)} \lambda(x)\, dx$ and so it is now dependent on the position, $\lambda(x)$. Eq. 2 models a transformation in which nuclei are located according to an inhomogeneous Poisson point process. Notice that the velocity is still a constant in Eq. 2. In the following section, we exemplify the difference between homogeneous and inhomogeneous Poisson in more detail.

Eq. 2 was compared with computer simulation using cellular automata [35] and using the causal cone method [30]. The agreement between the analytical model and the computer simulations was excellent.

The situation becomes much more complicated if one wished to generalize the velocity. A section below describes this situation in detail.

It is easier if one compares computer simulations using inhomogeneous nucleation with a constant velocity with computer simulations using homogeneous nucleation with inhomogeneous velocity [30]. Lyrio et al. [30] did this successfully in recent work.

In this paper, we go a step further. We compare computer simulations using inhomogeneous nucleation with a constant velocity with computer simulations in which both nucleation and velocity are inhomogeneous.

In this work, as in previous work, we combine computer simulation and analytical solutions. We believe that this combination is a powerful tool to understand microstructural evolution. Computer simulations can generate the microstructures as a function of time as well as permit the investigation of situations for which there is no analytical description.

2. Analytical description of inhomogeneous nucleation and position-dependent velocity

To derive an expression for the position-dependent velocity of an inhomogeneous velocity is much more complicated than for inhomogeneous nucleation.

The problem is that when the velocity is position independent, the shape of the growing region is spherical. However, for example, if one has a polymer crystalizing in a steep temperature gradient, the shape of the growing region does not remain spherical. A good illustration is in the work of Capasso et al. [14].

Nonetheless, if the gradient is not steep compared with the region size, it is possible to simplify the problem. For example, suppose a metal sheet 1 mm in thickness that has 90% deformation at the top and 10% deformation at the bottom. A reasonable grain size after recrystallization could be around 50 μm. The deformation gradient is (90-10)/1000 = 0.08%/μm. For a 50 μm grain, the change in deformation across its diameter would be equal to 4%. If the grain center is deformed 50%, then at the top,the grain will have a maximum deformation of 52% and, at the bottom, a maximum deformation of 48%. This 4% difference will be much less at the beginning of growth when the region is still small.

Under these circumstances, one may simplify the problem. One supposes that the point at which the grain nucleates determines the velocity, but each grain grows with a constant velocity. In this way, one has an inhomogeneous velocity, but an analytical solution is viable.

Following the above approach, Villa and Rios [26] proposed a simplified approach in which the growth velocity of each region was constant but depended on the coordinate of the nuclei from which the growth started. That is, $G(x)$ depends on the position of the nuclei in space but remains constant upon further growth so that the growing region remains spherical. In the present work, one used both a position-dependent/inhomogeneous growth velocity and inhomogeneous nucleation.

It is well known that $V_V(t, x)$ coincides with the probability that the point x belongs to the transformed region at time t. The so-called *causal cone* of a point x at time t, denoted here by $A(t, x)$, plays a fundamental role in evaluating $V_V(t, x)$. It is defined as the *region* (i.e., the subset of the space where the nucleation process N takes values) in which at least one nucleation event has to take place to cover the point x at time t; namely, by denoting with Θ^t the transformed region at time t, the following equivalence between events holds:

$$\{x \in \Theta^t\} \Leftrightarrow \{N(A(t,x)) > 0\}.$$

Consequently, if N is a Poisson process with intensity $\lambda = \lambda(y)$, then it directly follows by the probability law of the process that

$$V_V(t,x) = 1 - \exp\left\{-\int_{A(t,x)} \lambda(y)\, dy\right\}. \quad (3)$$

Under the assumptions above, the transformed region Θ^t at time t is given by

$$\Theta^t := \bigcup_{y \in N} B_{G(y)t}(y),$$

where $B_{G(y)t}(y)$ is the ball centered at point y with radius $G(y)t$, being $G(y)$ the growth velocity of a grain nucleated at $y = (y_1, y_2, y_3)$. Therefore, by the central symmetry of the grains,

$$A(t,x) = \left\{y \in \mathbb{R}^3 : x \in B_{G(y)t}(y)\right\} = \left\{y \in \mathbb{R}^3 : y \in B_{G(y)t}(x)\right\}$$

$$= \left\{y \in \mathbb{R}^3 : G(y)\, t \geq \sqrt{(y_1 - x_1)^2 + (y_2 - x_2)^2 + (y_3 - x_3)^2}\right\} \quad (4)$$

When the velocity is a constant, one can substitute $G(y)$ for G.

3. Computer simulation methodology

The nuclei were located within a 3D cubic matrix with 500 × 500 × 500 cubic cells. The matrix dimensions were 1 mm in length, height, and width. As a result, the simulated domain had a volume equal to 1 mm^3. For convenience, the units will be omitted in the text. Therefore, [0,1]x[0,1]x[0,1] corresponded to the axis (x_1, x_2, x_3). At the bottomöf the simulation volume: $x_3 = 0$, whereas at the top: $x_3 = 1$.

For a constant velocity, the simulation employed the causal cone method. This method has been employed in our previous works [36–39]. Fig. 1 illustrates the causal cone method for a site-saturated transformation. Fig. 1a shows a point " x " inside a ball of radius $R = Gt$ centered in x (solid line).The ball in Fig. 1a is the causal cone of point x at time t. The expression "causal cone" is used because when one considers time, one has a 4-D "cone" that has the ball of Fig. 1a as the "base" and the time as the "height." Whenever a nucleus is "captured" by this cone, the point x transforms. The ball in Fig. 1a contains no nuclei. Therefore, no growing region can overtake x within time t. As a result, x remains untransformed.

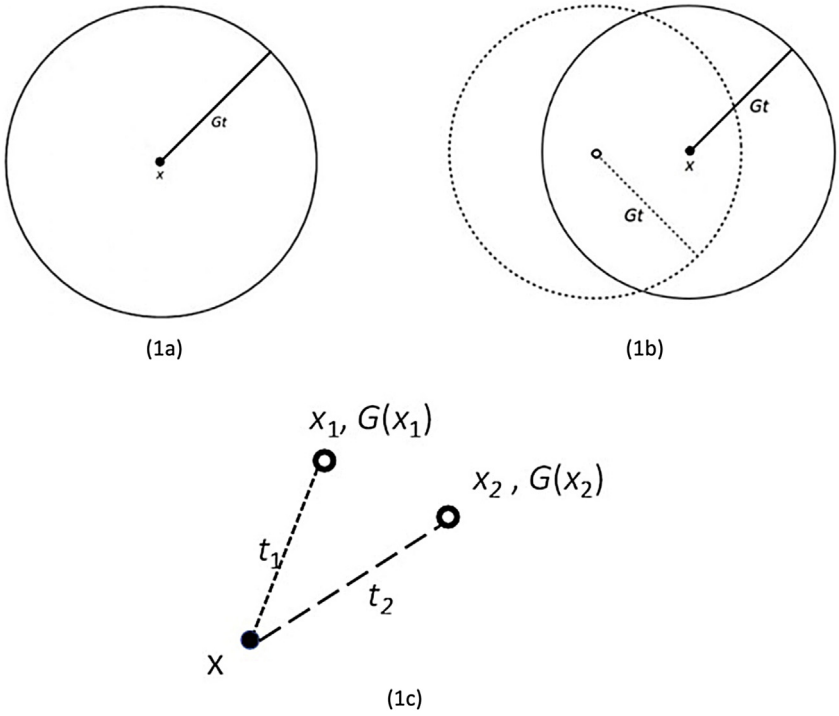

Fig. 1 – (1a) Fig. 1a shows a point *x* inside a ball of radius *R* = *Gt* centered in *x* (solid line). This ball is called the causal cone of *x*. No nuclei are inside this ball. Therefore, no transformed region can overtake *x* that remains untransformed. (1b) Fig. 1b shows a ball centered in *x* with one nucleus inside it. At time *t* the transformed region originated at the nucleus has grown to a ball of radius *R* = *Gt* (dashed line) encompassing the point *x* so that *x* is inside the transformed region. (1c) Fig. 1c shows a point *x* that can be transformed by two points x_1 or x_2. The point *x* is transformed by the transformed region that reaches *x* in the minimum time, t_1 or t_2.

By contrast, Fig. 1b shows an identical ball but containing one nucleus. At a specific time, *t*, the new region originated at the nucleus (dashed line) contained within the ball may grow and reach a radius = *Gt*. This ball of transformed region overtakes and transforms the point. In summary, to transform the point *x* at least one nucleus must be present within the ball centered in. Of course, this ball may contain more than one nucleus.

Unfortunately, the causal cone method, as described above, is not convenient when there is a velocity gradient. This is so because the shape of the causal cone, "A," described in Eq. 4, may be complicated. One wishes to keep the computer simulation as simple as possible. For this reason, we propose a technique, the smallest time method, that is akin to the causal cone. We propose that if two regions with different velocities growing from nuclei located at X_1 and X_2 can transform a certain point, then the nuclei that can reach *X* in the shortest time is chosen. More explicitly, if $\frac{X_1-X}{G(X_1)} = t_1 < \frac{X_2-X}{G(X_2)} = t_2$ then nucleus X_1 will transform the point. The smallest time method results in spherical regions growing with a constant velocity equal to the position of the nucleus that originated it, $G(X_1)$. This method ensures that the individual regions grow as spheres with constant velocity. Therefore, their growth coincides with the assumptions made on the derivation of the analytical solution, see above.

A limitation of the analytical solution is that it gives only the fraction transformed. In a computer simulation, one would like to generate the microstructure. The simulation must have a way to distinguish the growing regions or individual grains. For constant velocity, this is not a problem as we can associate a nucleus with the transformed region. The smallest time method also allows us to do this.

The problem with the smallest time method is that in contrast to the causal cone method employed to simulate a constant velocity, it does not have a sound mathematical basis. It is a method proposed based on our experience with simulating this kind of problem. Therefore, it would be desirable to have a criterion to guarantee that a given computer simulation is accurate. Fortunately, we do have such a criterion. The analytical solution is exact. Therefore, when the analytical solution coincides with the simulation result, it is a sure indication that the simulation is correct. This point will be taken up later in this paper.

All computer simulations for each specific condition were repeated 50 times. For example, the mean volume density displayed in the plots is the mean of the values obtained from 50 simulations. Of course, the microstructures depicted in the paper can only be obtained from one simulation.

Periodic boundary conditions were used along the x_1 and x_2 axes. By contrast, no periodic condition was applied to the x_3 axis. This was done because nuclei were located within the matrix according to an inhomogeneous Poisson point process with an intensity, $\lambda(x)$, varying along the direction x_3. The intensity was equal to $\lambda(x) = \lambda(x_1, x_2, x_3) = mx_3 + n$ where "*m*" and "*n*" are constants.

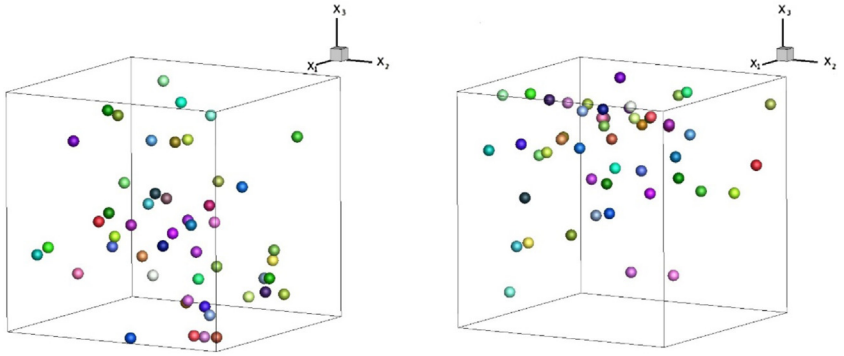

Fig. 2 – (2a) Realization of a homogenous Poisson point process with a constant intensity λ. The nuclei are homogeneously randomly located in space; (2b) Realization of an inhomogeneous Poisson point process with a position-dependent intensity $\lambda(x) = 96x_3 + 2$. The nuclei are inhomogeneously located in space along the x_3 direction. For example, for $x_3 = 0.75$ then $\lambda(0.75) = 74$ or for $x_3 = 0.25$ then $\lambda(0.25) = 26$.

Table 1 – Number of nuclei with their respective nuclei gradients and the different velocity gradients with their respective constant mean velocities.

Nuclei numbers	Gradient of nuclei	Velocity gradient	Constant velocity
1200	$\lambda(x) = 2396x + 2$	$G(x) = 0.1x + 0.2$	$G = 0.25$
4800	$\lambda(x) = 9596x + 2$	$G(x) = 0.3x + 0.2$	$G = 0.35$
19200	$\lambda(x) = 38396x + 2$	$G(x) = 1.0x + 0.2$	$G = 0.70$

Table 2 – Values of $\lambda(0.9)/\lambda(0.1)$ and $(G(0.9)/G(0.1))^3$ corresponding to $\lambda(x)$ and $G(x)$ shown in Table 1.

$\lambda(0.9)/\lambda(0.1)$	$(G(0.9)/G(0.1))^3$
9 (1200 nuclei)	2.6
9 (4800 nuclei)	8.5
9 (19200 nuclei)	49.3

Fig. 2 depicts an example of a homogeneous Poisson point process, no nuclei gradient, and a heterogeneous Poisson point process, with nuclei gradient. A point that might be confusing to the reader is that an inhomogeneous Poisson point process consists of discrete points, yet its intensity $\lambda(x)$ is continuous. The resolution of this apparent contradiction belongs to the realm of Stochastic Geometry. The detailed mathematical argument is beyond the scope of this work. For a full understanding of this point, it is necessary to check a Stochastic Geometry book, for example, ref. [40].

Similarly, the velocity varied along x_3 according to $G(x) = G(x_1, x_2, x_3) = ax_3 + b$ where "a" and "b" are constants. Table 1 contains the number of nuclei and well as the constants m, n, a, and b used in the computer simulations. For brevity, one will use x in the place of x_3 in what follows. In this work, nucleation was always site-saturated.

The choice of the constants in Table 1 followed a criterion defined as follows. If one observes Eq. 2 the coefficient of time is $\lambda(x)G^3$. The constants were chosen so that the ratio of number of nuclei per unit of volume, $\lambda(0.9)/\lambda(0.1)$ and $(G(0.9)/G(0.1))^3$ had comparable values. Table 2 shows that, for all cases, the ratio of $\lambda(0.9)/\lambda(0.1)$ was similar and equal to 9. Comparing $\lambda(0.9)/\lambda(0.1)$ with $(G(0.9)/G(0.1))^3$ for different velocity gradients, a good approximation between $\lambda(0.9)/\lambda(0.1)$ and $(G(0.9)/G(0.1))^3$ was observed for the gradient of $G(x) = 0.3x + 0.2$, as shown in Table 2. Thus, a relationship is observed between the number of nuclei gradient and the velocity gradient.

It is essential to point out that the nuclei gradients are the same for 1200, 4800, and 19200 nuclei. This can be seen dividing the slope of $\lambda(x)$ by the total number of nuclei: 2396/1200≅2, 9596/4800≅2. and 38396/19200≅2.

For the readers' convenience one can summarize the microstructural descriptors used here:

a) The mean volume density, $V_V(t, x)$, of the new phase; the mean interfacial area density, $S_V(t, x)$, between the new phase and the matrix.
b) The volume fraction transformed, $\mathbf{V_V}(t)$, is the integral of the mean volume density of the new phase over all the simulation volume, $\int_{[0,1]^3} V(t, x)\,dx$. Analogously, the interfacial area per unit of volume transformed, $\mathbf{S_V}(t)$, is the integral of the mean interfacial area density between the new phase and the matrix over all the simulation volume.
c) N_V is the number of grains per unit of volume.
d) The contiguity, $C_{\beta\beta}$, is defined as $C_{\beta\beta} = \frac{2S_V^{\beta\beta}}{S_V^{\alpha\beta} + 2S_V^{\beta\beta}}$, where β is a new phase, and α is the parent phase. $S_V^{\beta\beta}$ is the mean interfacial area density of the boundaries between the regions of the new phase and $S_V^{\alpha\beta}$ is the mean interfacial area density of the boundaries between the regions of the new phase and the parent matrix. Whereas in (a) and (b) one omitted the superscripts, here they were included for clarity. One may also define the contiguity in terms of the are per unit

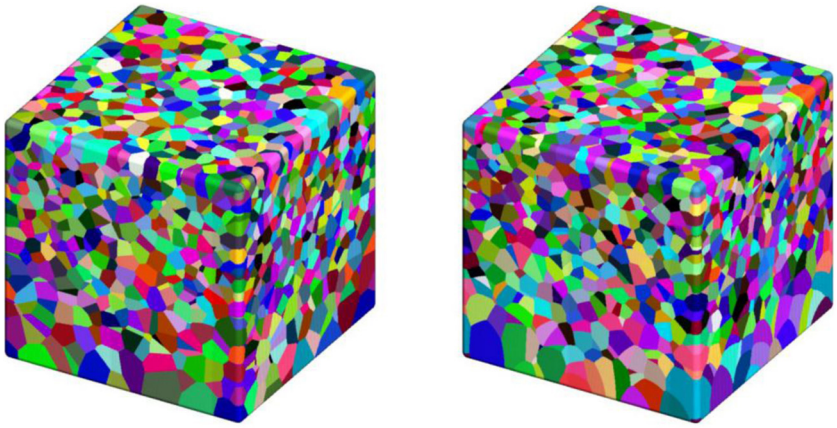

(3a) (3b)

Fig. 3 – 3D representation that shows the simulated microstructure with inhomogeneous nucleation and homogeneous growth velocity. Constant velocity and velocity gradient were compared. (3a) $G = 0.70$; (3b) $G(x) = 1.0x + 0.2$ for 4800 nuclei. The final grain size is smaller at the top than at the bottom in both cases. Both the nuclei gradient and the velocity gradient change only along the x_3 axis. In the figure, $x_3 = 0$ corresponds to the bottomänd $x_3 = 1$ to the top.

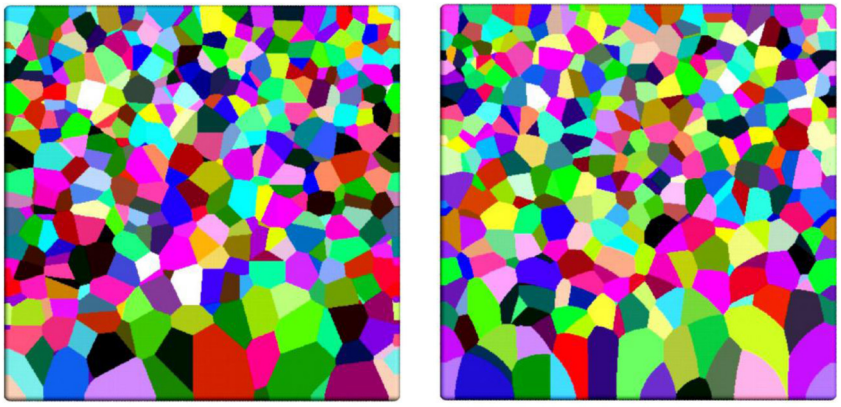

(4a) (4b)

Fig. 4 – 2D representation that shows the simulated microstructure with inhomogeneous nucleation and homogeneous growth velocity. Constant velocity and velocity gradient were compared. (4a)$G = 0.70$; (4b) $G(x) = 1.0x + 0.2$ for 4800 nuclei. The final grain size is smaller at the top than at the bottom in both cases.

of volume $C_{\beta\beta} = \frac{2S_V^{\beta\beta}}{S_V^{\alpha\beta}+2S_V^{\beta\beta}}$. The contiguity $C_{\beta\beta}$ is plotted as a function of the mean volume density, $V_V(t, x)$. The contiguity $C_{\beta\beta}$ is plotted as a function of the volume fraction, $V_V(x)$.

In what follows, the terms cönstant velocityänd homogenous velocityäs well as vëlocity gradientänd inhomogeneous velocityäre used as synonyms.

4. Microstructure

Figs. 3 and 4 compare the fully transformed microstructure when the nucleation is inhomogeneous and the velocity is homogeneous and inhomogeneous in 3D and 2D, respectively.

Visual inspection of Figs. 2 shows that the grains close to $x_3 = 1$, top of Fig. 2 are smaller than the grains close to $x_3 = 0$, the bottom of Fig. 2. Constant velocity and velocity gradient were compared. (2a) $G = 0.70$ and (2b) $G(x) = 1.0x + 0.2$ for 4800 nuclei.

By visual inspection, it is difficult to detect a difference between Figs. 3a and 3b, and Fig. 4a and 4b. They look similar, thus suggesting that the effect of a velocity gradient on the fully transformed microstructure is not substantial. This point will be taken up later in this paper.

Notice that for planes $x_3 =$ constant the microstructures are homogeneous within the planes. Compare, for instance, the planes $x_3 = 1$ in Figs. 3a and 3b.

Nonetheless, the microstructures do give clüesto distinguish between them. Figs. 4a and 4b show these clues better than Fig. 3a and 3b. In Fig. 4a, one can see that the grain

Fig. 5 – 2D section showing the microstructural evolution during transformation: left $V_V(t) = 0.1$, middle $V_V(t) = 0.3$, right $V_V(t) = 0.5$. The velocity was constant equal to 0.7 and the number of nuclei 4800.

Fig. 6 – 2D section showing the microstructural evolution during transformation: left $V_V(t) = 0.1$, middle $V_V(t) = 0.3$, right $V_V(t) = 0.5$. The velocity gradient was equal to $G(x) = 1.0x + 0.2$ and the number of nuclei 4800.

boundaries are straight. Straight grain boundaries are typical of site-saturated transformations. By contrast, Fig. 4b shows curved grain boundaries. This becomes especially apparent at the bottom of Fig. 4b. The authors found a similar effect in previous work [30]. In previous work, only the combination of velocity gradient and uniform randomly nucleation was studied. The velocity gradient results in a curved boundary because when the transformed regions impinge, the fastest-growing region will tend to envelop the slowest growing region.

Another visual difference, more subtle, is that the bottom grains in Fig. 4b appears to be more elongated than the bottom grains of Fig. 4a.

Therefore, when one compares the site-saturated microstructures side by side, the existence of curved boundaries is an indication that a velocity gradient might be involved.

Figs. 5 and 6 show the microstructural evolution in the first half of the transformation for constant velocity and a velocity gradient. The transformed volume fractions over the whole simulation volume are indicated.

The discrepancy between Figs. 5 and 6 is striking. The velocity gradient produces microstructures in which there is more transformation at the top than at the bottom when compared with microstructures generated by constant velocity.

Consequently, the microstructures diverge during transformation even though the fully transformed microstructures shown in Figs. 3 and 4 are similar.

Finally, it is interesting to compare the grain size measured on each plane when the transformation takes place with a constant velocity or with a velocity gradient. The total number of nuclei was the same in both cases: 4800. This is done in Fig. 7 for the fastest velocities simulated here, but the results were similar for lower velocities. Fig. 7 shows that there is a minor difference between the grain sizes of each plane in the fully transformed microstructure. This reinforces the similarity of the fully transformed microstructures already detected by visual inspection in Figs. 3 and 4.

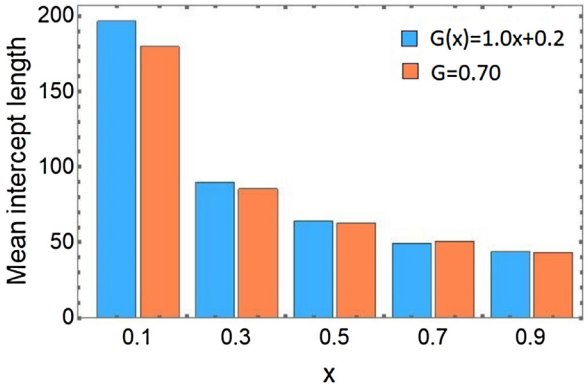

Fig. 7 – Grain sizes (mean intercept length) measured on each plane. The results are remarkably similar for the velocity gradient, $G(x) = 1.0x + 0.2$, and constant velocity equal to 0.7. The grain size for a velocity gradient is slightly larger than the grain size for a constant velocity on the plane closest to $x_3 = 0$, plane $x_3 = 0.1$.

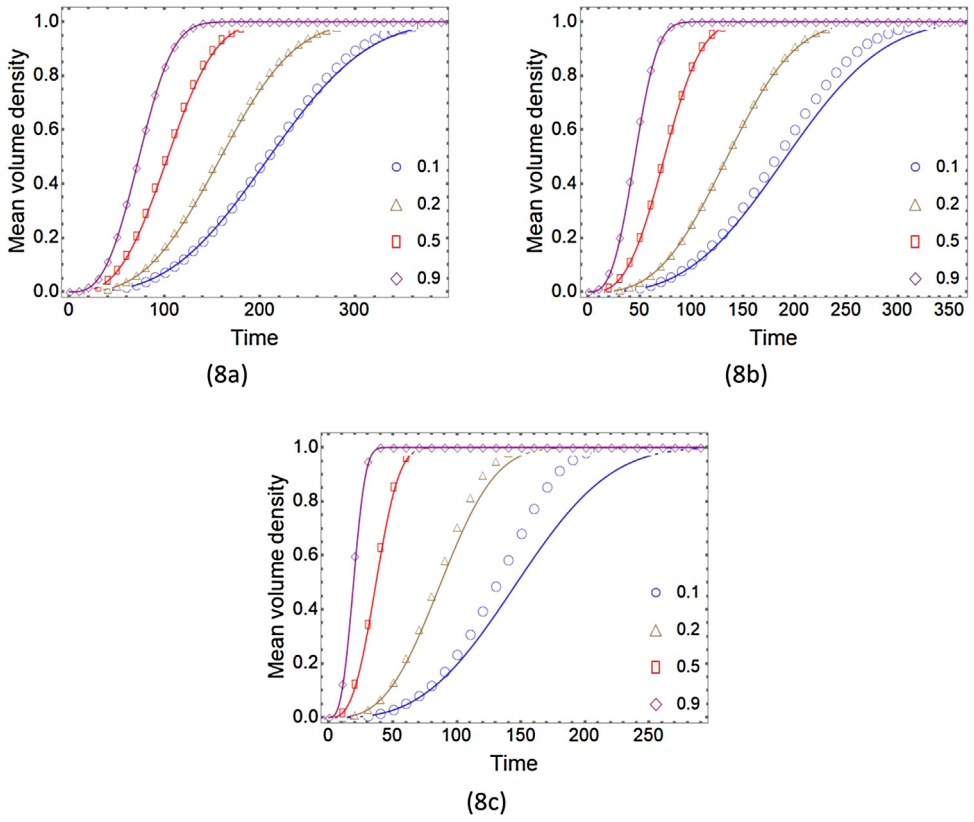

Fig. 8 – Transformation kinetics for inhomogeneous nucleation and inhomogeneous growth velocity. Different velocity gradients were compared. (8a) $G(x) = 0.1x + 0.2$; (8b) $G(x) = 0.3x + 0.2$ and (8c) $G(x) = 1.0x + 0.2$ for 1200 nuclei. Transformation kinetics, the mean volume density against time, is slower at the bottom that has a smaller growth velocity than at the top that has a high growth velocity. The dots represent the simulated data.

4.1. *Kinetics*

Figs. 8, 9 and 10 show the transformation kinetics on each plane. For each plane, Figs. 8,9 and 10 show the mean volume densities, $V_V(t, x)$, as a function of time for inhomogeneous nucleation and inhomogeneous velocity. Figs. 8,9, and 10 also show the influence of the total number of nuclei on the transformation.

Figs. 8a-c show the situation in which the matrix has a nuclei gradient of $\lambda(x) = 2396x + 2$ corresponding to 1200 nuclei. Different velocity gradients were compared: (8a) $G(x) = 0.1x + 0.2$; (8b) $G(x) = 0.3x + 0.2$ and (8c) $G(x) = 1.0x + 0.2$ for 1200 nuclei. Transformation kinetics, the mean volume density against time, is slower at the bottom because the velocity at the bottom is smaller than at the top. The solid lines represent the analytical results. The dots represent the simulated data. Fig. 8c depicts a noticeable deviation between the simulation and the analytical result for the plane closest to $x_3 = 0$, plane $x_3 = 0.1$.

Fig. 9 shows the situation in which the matrix has a nuclei gradient of $\lambda(x) = 9596x + 2$ corresponding to 4800 nuclei. Different velocity gradients were compared: (9a) $G(x) = 0.1x + 0.2$; (9b) $G(x) = 0.3x + 0.2$ and (9c) $G(x) = 1.0x + 0.2$. Transformation kinetics, the mean volume density against time, is slower at the bottom because the velocity at the bottom is smaller than at the top. The dots represent the simulated data. Fig. 9c depicts a slight deviation between the simulation and the analytical result.

Fig. 10 shows the situation in which the matrix has a nuclei gradient of $\lambda(x) = 38396x + 2$ corresponding to 19200 nuclei Different velocity gradients were compared: (10a) $G(x) = 0.1x + 0.2$; (10b) $G(x) = 0.3x + 0.2$ and (10c) $G(x) = 1.0x + 0.2$. Transformation kinetics, the mean volume density against time, is slower at the bottom because the velocity at the bottom is smaller than at the top. The dots represent the simulated data.

In most cases, the agreement between the analytical solution and computer simulation is excellent. The exception is Fig. 8c that depicts a noticeable deviation between the simulation and the analytical result for the plane closest to $x_3 = 0$, plane $x_3 = 0.1$. A smaller deviation is also observed in Fig. 9c. These deviations will be discussed below in the discussion section.

In summary, Figs. 8–10 show that the agreement between computer simulation and analytical solution improves for lower velocity gradients and a higher number of nuclei.

4.2. *Effect of inhomogeneous velocity on the transformation kinetics*

Another way of looking at the effect of the velocity gradient on the kinetics is to compare the transformation kinetics

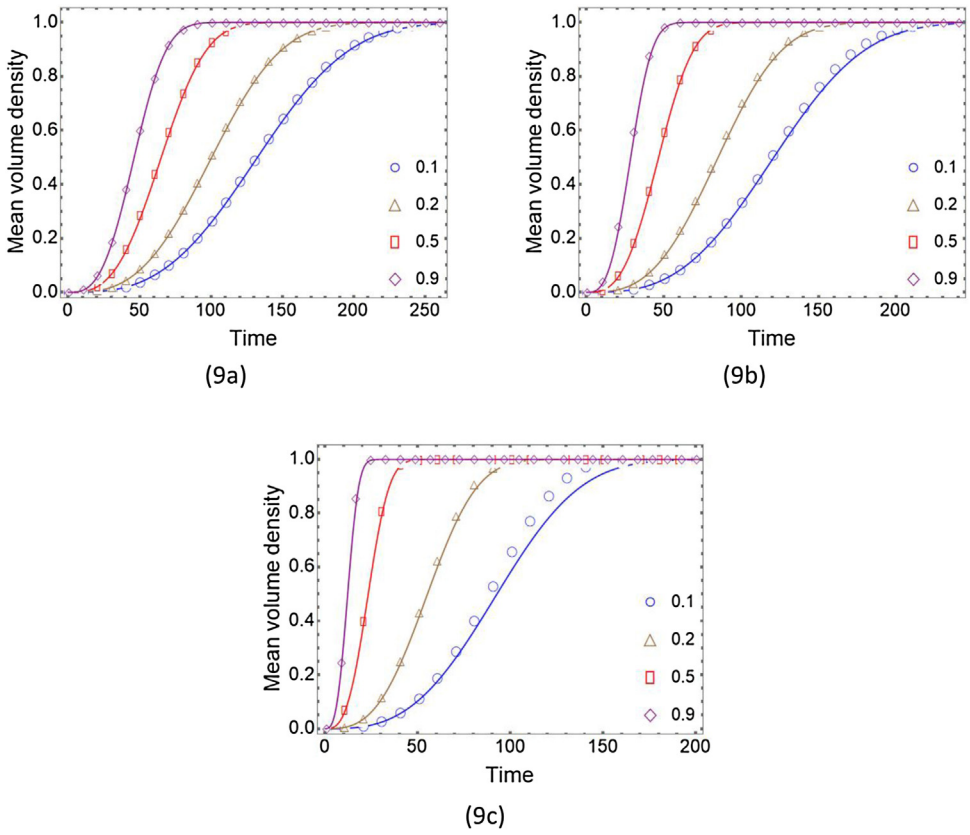

Fig. 9 – Transformation kinetics for inhomogeneous nucleation and inhomogeneous growth velocity. Different velocity gradients were compared. (9a) $G(x) = 0.1x + 0.2$; (9b) $G(x) = 0.3x + 0.2$ and (9c) $G(x) = 1.0x + 0.2$ for 4800 nuclei. Transformation kinetics, the mean volume density against time, is slower at the bottom that has a smaller growth velocity than at the top that has a high growth velocity. The dots represent the simulated data.

of two $x_3 =$ constant planes. One plane corresponding to 0.2 and another to $x_3 = 0.9$. Fig. 11 shows a comparison of transformation kinetics of $x_3 = 0.2$ and $x_3 = 0.9$ planes for inhomogeneous nucleation and inhomogeneous growth velocity with inhomogeneous nucleation with homogeneous velocity. The solid lines represent the results of the mean volume density of the planes for the velocity gradient. The points represent the results of the mean volume density of the planes for constant velocity. Different velocity gradients and constant velocities were compared. (11a) $G(x) = 0.1x + 0.2$; $G = 0.25$; (11b) $G(x) = 0.3x + 0.2$; $G = 0.25$ and (11c) $G(x) = 1.0x + 0.2$; $G = 0.70$ for 4800 nuclei. Likewise, one can see that the transformation kinetics, the mean volume density against time, at $x_3 = 0.2$ is slower than at $x_3 = 0.9$. Moreover, the growth velocity at $x_3 = 0.9$ is higher for a velocity gradient than for constant velocity. Conversely, the growth velocity at $x_3 = 0.2$ is lower for a velocity gradient than for constant velocity. At the bottom, $x_3 = 0.2$, the transformation kinetics with constant predominates over the transformation kinetics with a velocity gradient. The opposite is true at the top, $x_3 = 0.9$. This difference increases as the velocity gradient becomes steeper, see Figs. 11a to 11c.

4.3. *Contiguity for inhomogeneous nucleation and inhomogeneous velocity*

The contiguity characterizes the spatial arrangement of two phases — one phase, the new phase, nucleates within another phase, the parent matrix. When the nuclei are uniform randomly located within the parent phase, that is, when nuclei are located within the parent phase according to a homogeneous Poisson point process, there is an analytical expression for the contiguity as a function of volume transformed. [41,42]. The analytical line is useful as a reference line [43]. In the present case, when one measures the contiguity on a plane $x_3 =$ constant, the contiguity falls on this reference line. This result is independent of x_3 plane. This result is also independent of whether the velocity is a constant or if there is a velocity gradient.

Fig. 12 shows an example of this. Fig. 12 shows the contiguity for a situation in which both the nucleation and the velocity are inhomogeneous.

Instead of plotting the contiguity for each plane, one can plot the contiguity for the whole simulation volume. In this case, one must use the volume fraction and the area per unit

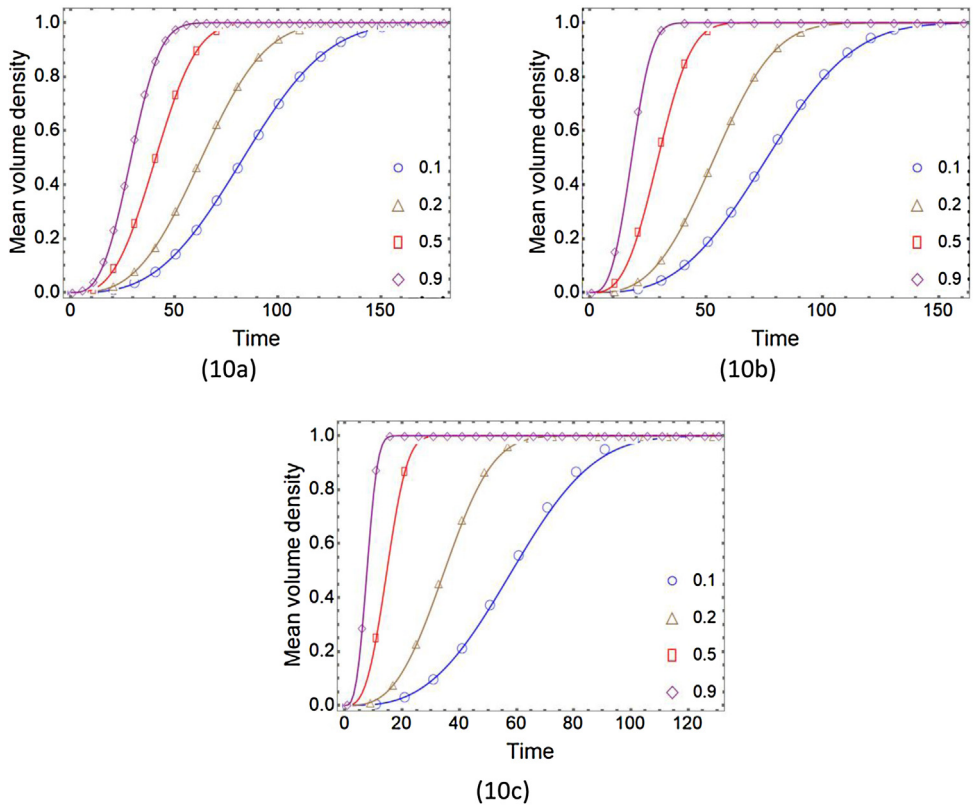

Fig. 10 – Transformation kinetics for inhomogeneous nucleation and inhomogeneous growth velocity. Different velocity gradients were compared. (10a) $G(x) = 0.1x + 0.2$; (10b) $G(x) = 0.3x + 0.2$ and (10c) $G(x) = 1.0x + 0.2$ for 19200 nuclei. Transformation kinetics, the mean volume density against time, is slower at the bottom that has a smaller growth velocity than at the top that has a high growth velocity. The dots represent the simulated data.

of volume of the interfaces of the new phase and the area per unit of volume of the interfaces between the new phase and the matrix.

Fig. 13 shows a comparison of the contiguity over the whole simulation volume for inhomogeneous nucleation and homogeneous growth velocity with inhomogeneous nucleation with inhomogeneous velocity. The solid line represents the analytical result. The dots represent the simulated data. Different velocity gradients and constant velocities were compared. (13a) $G(x) = 0.1x + 0.2$; $G = 0.25$ (13b) $G(x) = 0.3x + 0.2$; $G = 0.25$ and (13c) $G(x) = 1.0x + 0.2$; $G = 0.70$ for 4800 nuclei.

Fig. 13 shows that the contiguity of the constant velocity simulation falls between the contiguity of the velocity gradient simulation and the theoretical line.

Figs. 13a-c also show that the contiguity for constant velocity is independent of the number of nuclei. All the magenta dots in Figs. 13a-c fall in the same position. This is a direct consequence of the fact that the gradient of nuclei is the same for 1200, 4800, and 19200 nuclei. See Table 2.

5. Discussion

The first point to discuss is the validity of our simulation methodology. Figs. 8–10 illustrate this point. The simulation agrees with the theory very well except for the lowest number of nuclei and the plate located near the bottom of the simulation volume, $x_3 = 0.1$. The plane $x_3 = 0.1$ is the plane that is in a region that has a small number of nuclei. Therefore, the result suggests that for a smaller number of nuclei and a high-velocity gradient, the simulation does not work so well. A probable reason for that is that, for a small number of nuclei or large nuclei to nuclei distance, the high-velocity region may bypass the lower velocity region. So, if the simulation considers the smallest nucleus to X time, the high-velocity region may have a lower time, but owing to the need to bypass a transformed region in front of it, it may take a longer time to reach X than another region. Whatever the reason might be, the point is that when the simulation and analytical solution agree, one can trust the computer simulation.

One recalls the argument of the present authors in a previous paper concerning the effect of a velocity gradient on the microstructural inhomogeneity [30]. The microstructural inhomogeneity produced by an inhomogeneous velocity depends on the number of nuclei not only on the gradient itself.

A thought experiment might clarify this point. Consider a situation when one has only two nuclei one located at $x_3 = 0.75$ and another at $x_3 = 0.25$ along the central axis of the simulation volume. Suppose that the growth velocity of the transformed region nucleated at $x_3 = 0.75$ nucleus is three times the growth velocity of the region nucleated at the

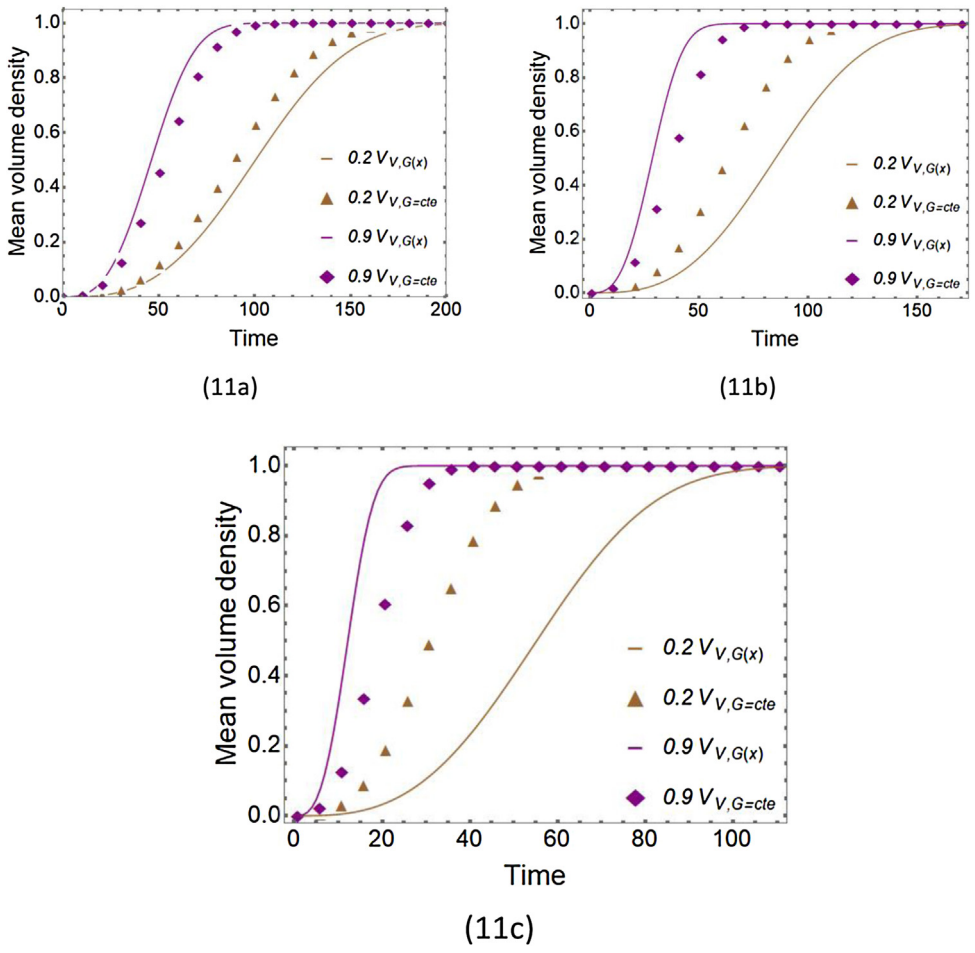

Fig. 11 – Comparison of transformation kinetics of 0.2 and 0.9 planes for inhomogeneous nucleation and inhomogeneous growth velocity with inhomogeneous nucleation with homogeneous velocity. Different velocity gradients and constant velocities were compared. (11a) $G(x) = 0.1x + 0.2$; $G = 0.25$; (11b) $G(x) = 0.3x + 0.2$; $G = 0.25$ and (11c) $G(x) = 1.0x + 0.2$; $G = 0.70$ for 4800 nuclei.

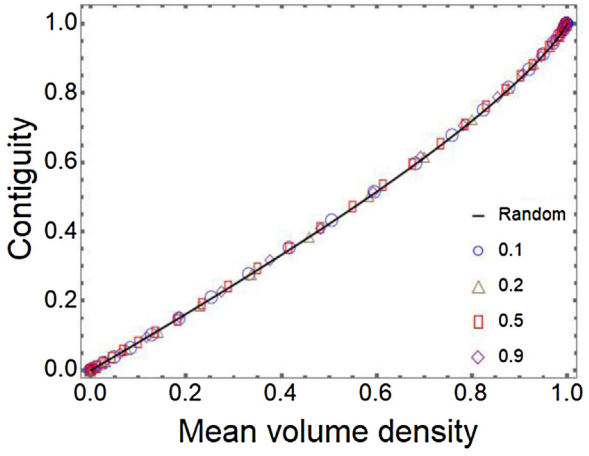

Fig. 12 – Contiguity x mean volume density for inhomogeneous nucleation and inhomogeneous growth velocity. The solid line represents the analytical result. The velocity is $G(x) = 0.3x + 0.2$ for 4800 nuclei. In the graph, the 0.1, 0.3, 0.5, 0.9 plans agree with the theoretical contiguity curve(solid line). The dots represent the simulated data.

$x_3 = 0.25$ nucleus. Thus, the grain resulting from the $x_3 = 0.75$ nucleus will be much larger than the grain resulting from the $x_3 = 0.25$ nucleus. In this case, the microstructural inhomogeneity caused by the difference in velocity is going to be high.

Consider now another situation when one has three nuclei one located at $x_3 = 0.75$, another at $x_3 = 0.50$ and another at $x_3 = 0.25$. The growth velocity of the transformed region nucleated at $x_3 = 0.75$ nucleus is three times the growth velocity of the region nucleated at the $x_3 = 0.25$ nucleus. Furthermore, suppose that the growth velocity of the transformed region nucleated at $x_3 = 0.50$ nucleus is twice the growth velocity of the region nucleated at the $x_3 = 0.25$ nucleus. In this situation, the presence of the transformed region nucleated at $x_3 = 0.50$ nucleus will inhibit the growth of transformed region nucleated at $x_3 = 0.75$. Consequently, the grain resulting from the $x_3 = 0.75$ nucleus will not be so much larger than the grain resulting from the $x_3 = 0.25$ nucleus, as in the previous case. In other words, the microstructural inhomogeneity will be less severe.

One can continue to add nuclei. For a high number of nuclei, it is reasonable to expect that the inhomogeneity owing to a

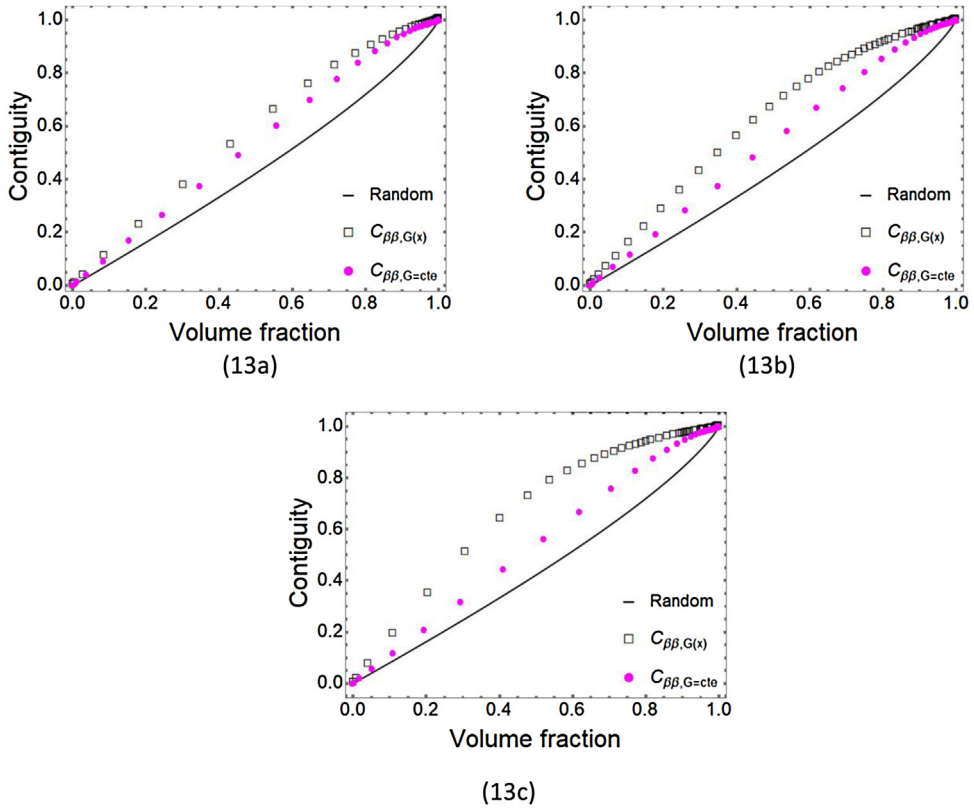

Fig. 13 – Comparison of the contiguity for inhomogeneous nucleation and homogeneous growth velocity with inhomogeneous nucleation with homogeneous velocity. The solid line represents the analytical result. Different velocity gradients and constant velocities were compared. (13a) $G(x) = 0.1x + 0.2$; $G = 0.25$ (13b) $G(x) = 0.3x + 0.2$; $G = 0.25$ and (13c) $G(x) = 1.0x + 0.2$; $G = 0.70$ for 4800 nuclei.

velocity gradient to be small. This behavior was also observed in a previous paper [26], where nuclei were uniform randomly located within the matrix. An analogous situation takes place here, even though one has nuclei located according to an inhomogeneous Poisson point process. Fig. 6 illustrates this. For the number of nuclei used here 1200, 4800, and 19200, the effect of the velocity gradient on the final microstructure was small. To relate these numbers to practical applications, one may consider that the edge of the simulation cube has 1 mm. Supposing that the grains are spherical with radius, R, the volume is $= \frac{4\pi R^3}{3}$. The grain size (mean intercept length) is 4R/3. Therefore, the mean grain sizes in the simulation range from about 80 μm (for 1200 nuclei) to 30 μm (for 19200 nuclei). This range is a typical practical range of grain sizes. If the number of nuclei is further increased, one gets even smaller grain sizes, and the trend indicates that the simulation and analytical solution will continue to agree.

Finally, even though the difference between the final microstructures was not significant, there is one point that may be used to distinguish them. As mentioned above, the grain boundaries are straight when the velocity is a constant but are curved when there is a velocity gradient, see Figs. 3 and 4.

Based on our results, a velocity gradient does not appear to have a considerable influence upon the final microstructure. By contrast, a velocity gradient has a substantial effect on the microstructural evolution and transformation kinetics. Figs. 5 and 6 illustrate the effect of a velocity gradient on the microstructural evolution. When a velocity gradient is present, the transformation at the top is faster than at the bottom. By contrast, for constant velocity, the transformation is more uniform. Notice that the inhomogeneity is due to the underlying nuclei being located according to an inhomogeneous Poisson point process.

The kinetics reflects microstructural evolution. Fig. 11 clearly shows this. The transformation on the plane $x_3 = 0.2$ is much faster for a constant velocity than for a velocity gradient because, of course, the velocity gradient has a much slower velocity $x_3 = 0.2$. By contrast, for $x_3 = 0.9$ the velocity gradient has a much faster velocity than the constant velocity.

Another interesting parameter is the contiguity, see the Methodology section for its definition. The contiguity measures the impingement of the interfaces of the transformed regions relative to the total interfacial area density.

The contiguity of constant velocity transformation is closer to the theoretical line than the contiguity of velocity gradient transformation. Fig. 12 shows the contiguity for a situation in which both the nucleation and the velocity are inhomogeneous. In Fig. 12, the solid line represents the analytical result for the situation in which nuclei are uniform randomly located in space, i. e., homogeneous Poisson point process. In the graph, the 0.1, 0.3, 0.5, 0.9 plans agree with the theoretical

contiguity curve(solid line). The dots represent the simulated data. This means that on each plane, the nuclei are randomly located, as expected from a Poisson point process.

More interesting is to plot the interfacial area density integrated over the whole simulation volume, that is, the area per unit of volume. $S_V^{\beta\beta}$ and $S_V^{\alpha\beta}$, against the volume fraction transformed over the whole simulation volume, V_V. Fig. 14 shows a comparison of the contiguity over the whole simulation volume for inhomogeneous nucleation and homogeneous growth velocity with inhomogeneous nucleation with homogeneous velocity. The solid line represents the analytical result. The dots represent the simulated data.

The contiguity of constant velocity transformation is closer to the theoretical line than the contiguity of velocity gradient transformation. Vandermeer [43] proposed that when the contiguity curve is above the theoretical curve, this points to clustering. When one looks at Figs. 5 and 6, one understands what is happening. When there is a velocity gradient, for the same total volume fraction, one can see a high fraction transform on the upper regions of the simulation sample. When the velocity is constant, the transformation is more spread. Therefore, the effect of clustering here means a higher fraction transformed at the top of the simulation volume. Consequently, one might expect the contiguity over the whole volume of the velocity gradient transformation to be above the transformation over the whole simulation volume of a constant velocity. Moreover, one sees that this trend is enhanced form Fig. 13a to Fig. 13c as one has a steeper velocity gradient.

6. Summary and conclusions

In this work, we conducted a computer simulation in which there was an inhomogeneous nuclei density. One compared the situation in which one has a constant velocity with the situation in which one has an inhomogeneous growth velocity. The computer simulation results were compared with exact analytical solutions available for each case. The main conclusions are:

- For the range of velocity gradients and the number of nuclei used here, all computer simulations showed good agreement with the analytical model of Rios and Villa [24,26].
- The exact solution may be used to check whether computer simulation is accurate or not for a given velocity gradient and the number of nuclei. For a constant velocity, the analytical solution was in good agreement with all simulations. When the velocity was inhomogeneous, one must choose a total number of nuclei sufficiently high for the employed velocity gradients. When the number of nuclei is too small, the computer simulation may not agree with the analytical solution, for reasons explained in the text.
- A velocity gradient significantly changes the transformation kinetics and microstructural evolution compared with a constant velocity. However, for the number of nuclei and velocity gradients used here, the final microstructures were similar. One significant difference is that a velocity gradient produces a final microstructure that has curved grain boundaries. By contrast, a constant growth velocity produces a final microstructure that has straight grain boundaries.

Authors agreement

I certify that all authors have seen and approved the final version of the manuscript being submitted. This article is the authors' original work, hasn't received prior publication and isn't under consideration for publication elsewhere.

This paper is based on the paper presented during ABM Week 2019 entitled "Simulação computacional de transformações com nucleação e velocidade não homogêneas". The ABM Week paper has been entirely rewritten, the title and author order changed and more material was added in order to meet JMRT standards.

Conflicts of interest

The authors declare no conflicts of interest.

Acknowledgments

This study was financed in part by the Coordenação de Aperfeiçoamento de Pessoal de Nível Superior - Brasil (CAPES) - Finance Code 001. The authors are grateful to Conselho Nacional de Desenvolvimento Científico e Tecnológico, CNPQ and Fundação de Amparo à Pesquisa do Estado do Rio de Janeiro, FAPERJ, for the financial support. The authors gratefully acknowledge the Center for Computational Materials Science, Institute for Materials Research, Tohoku University for the use of MASAMUNE-IMR(MAterials science Supercomputing system for Advanced MUlti-scale simulations towards Next-generation-Institute for Materials Research) supercomputer. In particular, the authors are grateful to Profs. Yayoi Terada and Tetsuo Mohri for their collaboration through the Global Institute for Materials Research Tohoku (GIMRT) program.

REFERENCES

[1] Kolmogorov AN. On the statistical theory of metal crystallization. Izv Akad Nauk USSR-Ser Matemat 1937;1:355–9.
[2] Johnson WA, Mehl RF. Reaction kinetics in processes of nucleation and growth. Trans AIME 1939;135:416–41.
[3] Avrami MJ. Kinetics of phase change. I general theory. J Chem Phys 1939;7:1103–12.
[4] Avrami MJ. Kinetics of phase change. II transformation-time relations for random distribution of nuclei. J Chem Phys 1940;8:212–24.
[5] Avrami MJ. Granulation, phase change, and microstructure kinetics of phase change. III. J Chem Phys 1941;9:177–84.
[6] Wang D, Liu Y, Zhang Y. Improved analytical model for isochronal transformation kinetics. J Mater Sci 2008;43:4876–85.
[7] Liu YC, Sommer F, Mittemeijer EJ. Austenite–ferrite transformation kinetics under uniaxial compressive stress in Fe–2.96 at.% Ni alloy. Acta Mater 2009;57:2858–68.

[8] Liu YC, Sommer F, Mittemeijer EJ. Abnormal austenite–ferrite transformation behaviour in substitutional Fe-based alloys. Acta Mater 2003;51:507–19.
[9] Vandermeer RA, Jensen DJ. Microstructural path and temperature dependence of recrystallization in commercial aluminum. Acta Mater 2001;49:2083–94.
[10] Rios PR, Yamamoto T, Kondo T, Sakuma T. Abnormal grain growth kinetics of BaTiO3 with an excess TiO2. Acta Mater 1998;46:1617.
[11] Kondo T, Sakuma T, Rios PR. Application of microstructural path analysis to abnormal grain growth of BaTiO3 with an excess TiO2. Scripta Mater 1998;39:1713–7.
[12] Rios PR, Guimarães JRC. Microstructural path analysis of athermal martensite. Scripta Mater 2007;57:1105–8.
[13] Rios PR, Guimarães JRC. Formal Analysis of Isothermal Martensite Spread. Mater Res 2008;11:103.
[14] Capasso V, Burger M, Micheletti A, Salani C. Mathematical models for polymer crystallization processes. In: Capasso V, editor. Mathematical modelling for polymer processing. Mathematics in industry 2. Berlin Heidelberg: Springer-Verlag; 2003. p. 167–242.
[15] Barbosa OX, Assis WLS, Garcia VS, Alvarez GB. Computational simulation of gliomas using stochastic methods. Research and Teaching in Exact and Natural Sciences 2019;3(2):199–215.
[16] Barmak K. A Commentary on: R̈eaction Kinetics in Processes of Nucleation and Growth:̈ Metallurgical and Materials Transactions 2010;41:2711–75.
[17] Guimarães JRC, Rios PR, Alves ALM. An Alternative to Avrami Equation. Mater Res 2019;22(5):e20190369.
[18] Liu F, Sommer F, Bos C, Mittemeijer EJ. Analysis of solid state phase transformation kinetics: model and Recipes. Int Mater Rev 2007;52(4):193–212.
[19] Song SJ, Liu F, Jiang YH, Wang HF. Kinetics of solid-state transformation subjected to anisotropic effect: model and application. Acta Mater 2011;59:3276–86.
[20] Song SJ, Liu F, Jiang YH. An analytic approach to the effect of anisotropic growth on diffusion-controlled transformation kinetics. J Mater Sci 2012;47:5987–95.
[21] Liu F, Yang CL, Yang GC, Li JS. Deviations from the classical Johnson–Mehl–Avrami kinetics. J Alloys Compd 2008;460:326–30.
[22] Liu F, Liu XN, Wang Q. Examination of Kissinger's equation for solid-state transformation. J Alloys Compd 2009;473:152–6.
[23] Liu F, Nitsche H, Sommer F, Mittemeijer EJ. Nucleation, growth and impingement modes deduced from isothermally and isochronally conducted phase transformations: Calorimetric analysis of the crystallization of amorphous Zr50Al10Ni40. Acta Mater 2010;58:6542–53.
[24] Rios PR, Villa E. Transformation kinetics for inhomogeneous nucleation. Acta Mater 2009;57:1199–208.
[25] Rios PR, Villa E. Application of stochastic geometry to nucleation and growth transformations. In: Molodov DA, editor. Microstruct. Des. Adv. Eng. Mater. first ed. Weinheim-Germany: Wiley-VCH; 2013. p. 119–59.
[26] Villa E, Rios PR. On modelling recrystallization processes with random growth velocities of the grains in materials science. Image Anal. Stereol 2012;31:149–62.
[27] Ohno M, Yamaguchi T, Sato D, Matsuura K. "Existence or nonexistence of thermal pinning effect in grain growth under temperature gradient,". Comput Mater Sci 2013;69:7–13.
[28] Song X, Rettenmayr M, Muller C, Exner HE. Modeling of recrystallization after inhomogeneous deformation. Met. Trans 2001;32A:2001–199.
[29] Song X, Rettenmayr M, Liu G. 3D Simulation study of inhomogeneous microstructure and its evolution (advantages of visual simulation technique in stereological analysis). Image Anal Stereol 2003;22:163–9.
[30] Lyrio MS, Alves ALM, Sá GMS, Ventura HS, Assis WLS, Rios PR. Comparison of transformations with inhomogeneous nucleation and transformations with inhomogeneous growth velocity. J Mater Res Technol 2019;8(5):4682–6.
[31] Song X, Rettenmayr M. Study on the effects of a deformation gradient on recrystallization in a material containing precipitates. Scripta Mater 2003;48:1123–8.
[32] Wang X, Huang Z, Cai B, Zhou N, Magdysyuk O, Gao Y, et al. Formation mechanism of abnormally large grains in a polycrystalline nickel based superalloy during heat treatment processing. Acta Mater 2019;168:287–98.
[33] Miller VM, Johnson AE, Torbet CJ, Pollock TM. Recrystallization and the Development of Abnormally Large Grains After Small Strain Deformation in a Polycrystalline Nickel-Based Superalloy. Metall. Mater. Trans. A Phys. Metall. Mater. Sci 2016;47(4):1566–74.
[34] Zambaldi C, Roters F, Raabe D, Glatzel U. Modeling and experiments on the indentation deformation and recrystallization of a single-crystal nickel-base superalloy. Mater. Sci. Eng. A 2007;454–455:433–40.
[35] Rios PR, Jardim D, Assis WLS, Salazar TC, Villa E. Inhomogeneous Poisson point process nucleation: comparison of analytical solution with cellular automata simulation. Mater Res 2009;12:219–24.
[36] Alves ALM, Assis WLS, Rios PR. Computer simulation of sequential transformations. Acta Mater 2017;126:451–68.
[37] Alves ALM, Villa E, Rios PR. Transformation kinetics for nucleation on second-phase particles: analytical solution and computer simulation. Acta Mater 2017;131:523–33.
[38] Sá GMS, Lyrio MS, Alves ALM, Ventura HS, Assis WLS, Rios PR. Generalizing ellipsoidal growth. Mater Res 2019;22(3):1–8.
[39] Ventura HS, Sá GMS, Duarte ACL, Assis WLS, Rios PR. Original Article Computer simulation in 3D of a phase transformation nucleated by simple sequential inhibition process. J Mater Res Technol 2020;9(1):152–61.
[40] Chiu SN, Stoyan D, Kendall WS, Mecke J. Stochastic geometry and its applications. 3rd ed. Chichester - United Kingdom: Wiley; 2013.
[41] Rios PR, Godiksen RB, Schmidt S, Juul Jensen D, Vandermeer RA. Analytical expression for the evolution of interfacial area density between transformed grains during nucleation and growth transformations. Scr Mater 2006;54:1509–13.
[42] Rios PR, Pereira LO, Oliveira FF, Assis WLS, Castro JA. Impingement function for nucleation on non-random sites. Acta Mater 2007;55:4339–48.
[43] Vandermeer RA. Microstructural descriptors and the effects of nuclei clustering on recrystallization path kinetics. Acta Mater 2005;53:1449–57.